Sensors & Actuators: B. Chemical 301 (2019) 127067

Contents lists available at ScienceDirect

Sensors and Actuators B: Chemical

journal homepage: www.elsevier.com/locate/snb

Plasma assisted formation of 3D highly porous nanostructured metal oxide network on microheater platform for Low power gas sensing

Hu Long[a,b,c,d], Sally Turner[a,b,c,e], Aiming Yan[a,h], Hongmei Xu[f], Moonsuk Jang[a], Carlo Carraro[d,g], Roya Maboudian[d,g], Alex Zettl[a,b,c,*]

[a] Department of Physics, University of California, Berkeley, California 94720, USA
[b] Materials Science Division, Lawrence Berkeley National Laboratory, Berkeley, California 94720, USA
[c] Kavli Energy NanoSciences Institute at the University of California, Berkeley and the Lawrence Berkeley National Laboratory, Berkeley, California 94720, USA
[d] Berkeley Sensor & Actuator Center, University of California, Berkeley, California 94720, USA
[e] Department of Chemistry, University of California, Berkeley, California 94720, USA
[f] University of Chinese Academy of Sciences, Beijing, China
[g] Department of Chemical and Biomolecular Engineering, University of California, Berkeley, California 94720, USA
[h] Department Physics, University of California, Santa Cruz, California 95064, USA

ARTICLE INFO

Keywords:
Gas sensor
Microheater
Metal oxide
Oxygen plasma
Formaldehyde

ABSTRACT

A facile and versatile approach that integrates highly porous metal oxide nanostructured network with a low power microheater platform is presented for the creation of low-power, miniaturized gas sensors. Highly porous nanostructured metal oxide network is formed by oxygen plasma treatment of a metal containing polymer film followed by a heat treatment. A generalized aqueous metal precursor solution allows a large variety of metal salts to be incorporated into cast polymer films, thus forming nanostructured metal oxide network with various compositions. Gas sensing behavior is demonstrated for Co_3O_4 -based devices, exhibiting high sensitivity, low detection limit, and fast response and recovery towards formaldehyde gas. The overall fabrication process is flexible and highly scalable. This facile and flexible fabrication method can be used to reproducibly fabricate a variety of low power gas sensors with tunable performances for many applications and has great potential for mass production.

1. Introduction

The demand for compact, low-power gas sensors is rapidly expanding [1–6]. Sensors integrated into smartphones, other mobile sensor platforms, or even wearables, require gas sensors with small size, low power consumption, and low cost. Unfortunately, most commercially available gas sensors are still bulky and consume high power (> 50 mW) [2,7,8]. Development of low-power chip-scale gas sensors with acceptable performance is critical for many applications utilizing battery, solar, or other local energy harvesting sources [8–11].

Semiconducting metal oxide sensors are among the most popular and promising solid-state chemical sensors due to their high stability, low cost, and large variety of metal oxides available [12–14]. However, metal oxides typically require high temperature (> 200 °C) to achieve good sensitivity and reasonable response and recovery. As the heating elements paired to metal oxides consume most of the power and define the sensor size, low power consumption and sensor miniaturization can be simultaneously accomplished by using a microheater platform [6,8–11,15–18]. A thermally insulated microheater platform can leverage silicon micromachining processes to achieve scalable, low cost and reproducible manufacturing.

However, sensor miniaturization also significantly decreases the active area available for sensing, which can in turn lead to poor sensitivity. High surface area nanomaterials such as nanoparticles, nanowires, and hierarchical nanostructures can be used to compensate for the reduced sensing footprint [12,19]. The integration of nanomaterials into a microheater platform remains a significant challenge. The most popular strategy, inkjet printing, requires sophisticated ink preparation to prevent clogging of the injecting nozzle, since nanomaterials generally aggregate heavily in solution [20–24]. During film formation and sensor operation, nanomaterials can aggregate when surfactants and solvent are removed, leading to a loss in active surface area. In addition, the printing process requires the direct contact of the nozzle and membrane, which may break the suspended membrane. There remains

---

* Corresponding author.
E-mail address: azettl@berkeley.edu (A. Zettl).

https://doi.org/10.1016/j.snb.2019.127067
Received 4 June 2019; Received in revised form 7 August 2019; Accepted 30 August 2019

a need for a simple, flexible method for the synthesis of metal oxide nanomaterials with well-defined porous structure that can be easily implemented on-chip and used to effectively fabricate highly integrated miniaturized gas sensors.

In this paper, we present a versatile strategy for the fabrication of high-performance gas sensors through plasma assisted on-chip synthesis of highly porous metal oxide nanostructured network on a low power microheater platform. Vertically aligned and interconnected metal oxide network, including those based on Co_3O_4, NiO, and SnO_2, are created by oxygen plasma treatment of cast polymer films followed by additional heat treatment. As a demonstration, the sensing performance of a Co_3O_4-based sensor is established, showing high sensitivity and selectivity toward formaldehyde, with extremely fast response and recovery times. The simplicity, flexibility, and controllability of our preparation method enable the fabrication of a versatile class of gas sensors with high sensitivity, fast response and recovery, and tunable selectivity toward specific gases depending on their constituent metal oxide sensing material(s).

2. Results and discussion

Fig. 1 schematically illustrates the sensor fabrication process. A generalized metal precursor aqueous solution is prepared by dissolving metal salts in a water-based polyvinyl alcohol (PVA) solution (10%). Using a water soluble polymer enables the selection of large variety of metal salts [25]. The precursor solution is spin-coated onto a substrate to form a homogenous metal-precursor-containing polymer film. The PVA film is subsequently plasma etched and heat treated. The plasma etching controls the final network thickness, and the heat treatment creates pores in the nanostructures, beneficial for gas sensing.

For gas sensing applications, the above-mentioned film is an integral part of a microheater platform consisting of a polycrystalline silicon carbide (SiC) heater embedded in a suspended low-stress silicon nitride (LSN) membrane anchored to a Si frame. The microheater provides the thermal energy to activate the sensing reaction (Fig. 2). The detailed fabrication process of the microheater can be found in our prior reports [9,10]. The microheater platform is 3.5 × 3.5 mm^2 in size with four heater elements in a single chip (Fig. 2a). Fig. 2b and c show zoomed-in optical images of a single heater where the two sensing electrodes (yellow color) are above the SiC heater (green color) separated by the LSN membrane. The gap between two sensing electrodes is 2 µm. The heating area is around 50 × 50 μm^2. The suspended thin membrane design thermally isolates the microheater from the frame and minimizes power consumption, requiring only 5.6 mW input power to reach 200 °C, as shown in Fig. 2d.

To convert the metal-ion-containing polymer film (integrated with the microheater) into a functioning sensor element, the entire microheater/sensor platform is treated by oxygen plasma to convert the film to a metal-containing nanostructured network. The metal-containing polymer nanostructured network is then annealed at 500 °C in air for 2 h, using either the microheater itself, or in a tube furnace whereby the entire platform is heated. The annealing step removes the polymer and converts the metal precursor to metal oxide. The polymer removal during annealing also creates mesopores in the nanostructures, which is another benefit of using PVA. Annealing by the microheater allows the in-situ localized formation of metal oxide nanostructures on the heated area only (Fig. S1). The sensor substrate can be further washed by hot water to remove polymer remaining on the unheated regions of the chip.

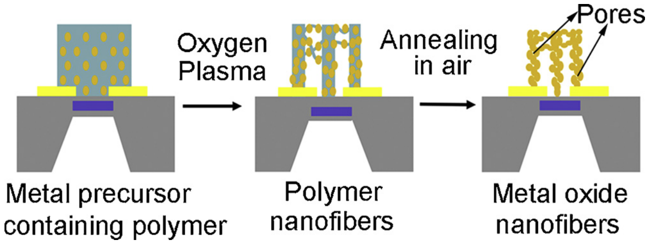

Fig. 1. Schematic of the sensor fabrication process.

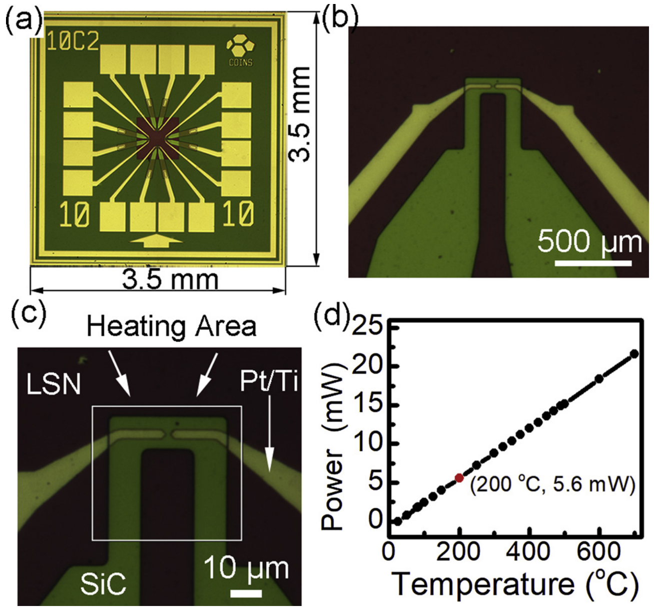

Fig. 2. (a) Optical image of a chip consisting of four SiC microheaters (3.5 × 3.5 mm2); (b) enlarged optical image of one microheater (dark green), also showing the sensing electrodes (light green); (c) optical image of the heating area of microheater; (d) relationship between microheater power and temperature of the microheater (For interpretation of the references to colour in this figure legend, the reader is referred to the web version of this article).

Conversions to a polymer nanofiber array upon oxygen plasma etching have been discussed previously in the literature [26–31]. It is suggested that the formation mechanism of the nanostructured network relies on the directionality of the plasma etching combined with the self-masking effect brought by the metal impurities in the polymer [29,31]. The ratio between PVA and metal salts can be tuned to obtain the desired nanostructure morphology (Fig. S2). If the metal ratio is too low, the density of the network is low as well, resulting in a non-continuous conductive path. If the metal ratio is too high, the resulting film will be a dense film with a low surface area. The polymer film to nanofiber array conversion process affords great flexibility and provides good control over the ultimate sensor element morphology. For example, the density of the nanostructured network can be further tuned by the ratio of PVA in water, and the baking temperature and time before plasma treatment.

Fig. 3 shows representative scanning electron microscopy (SEM) images at various magnifications of an as-prepared Co_3O_4 nanostructured network on the microheater chip. Similarly prepared NiO, and SnO_2 nanostructured networks are shown in Fig. S3. As shown in the low magnification SEM images in Fig. 3(a) and (b), the nanofibers are uniformly distributed across the whole heated area. The nanostructured networks have maintained their shapes with no signs of collapsing, indicating the robustness of the structure. Based on the high-resolution SEM image in Fig. 3(c), the nanostructured network is highly porous, with pore size ranging from 20 to 500 nm. The nanofibers appear well-interconnected, which enhances both their electrical conductivity and mechanical stability. Fig. 3(d) shows a side view of the nanostructured Co_3O_4 network. The nanostructured network has uniform height of around 550 nm. The fibers are connected at the top, forming conductive paths, while the pores between the fibers are abundant and highly accessible to gases.

Fig. 4 presents low magnification transmission electron microscopy

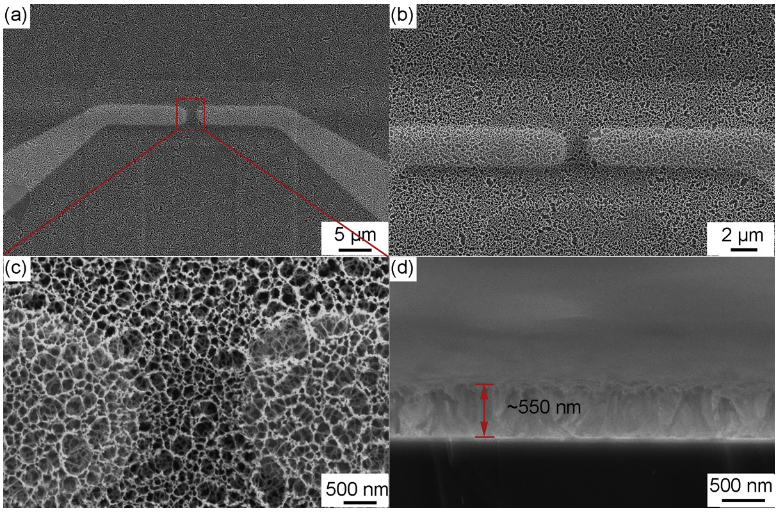

Fig. 3. (a–c) top-down SEM images of the nanostructured Co_3O_4 network on microheater chip with different magnifications. (d) Side view SEM image of the nanostructured Co_3O_4 network on a Si (100) chip with the same synthesis conditions.

(TEM) images, further showing the porous characteristic of the nanostructured network, in good agreement with SEM observation. Fig. 4b shows the side view of nanostructured Co_3O_4 network, where the directional nanofibers can be seen. The nanofibers are interconnected with each other forming porous walls, which are made up of small nanoparticles, as shown in Fig. 4c-d. The average size of the particles is around 5 nm. Smaller particles are favorable for gas sensing applications due to the increased surface-to-volume ratio as well as the increased number of grain contacts in the conductive sensing path. In addition, numerous inter-particle pores with diameter of 1–4 nm are found in the structure during the annealing step for removing the polymers. Hierarchical porosity, as observed here, is highly desirable as the pores enhance the response and recovery rates of the sensor during operation due to enhanced gas permeability. From Fig. 4d, a lattice spacing of 0.47 nm is observed in the individual nanoparticles, consistent with the (111) plane of the Co_3O_4.

X-ray diffraction (XRD) is conducted to identify the composition and crystalline phases of the nanostructured Co_3O_4 network. Fig. 5 shows the XRD pattern of the as-prepared nanostructured Co_3O_4 network. All the diffraction peaks can be indexed to the spinel structure of Co_3O_4, which matches well with JCPDS Card No. 73-1701. No other peaks corresponding to other materials are observed in the XRD pattern, indicating the complete transformation of Co ions to Co_3O_4. X-ray photoelectron spectroscopy is used to further characterize the surface composition of the hierarchical Co_3O_4 structure. Fig. S4 shows the high resolution XPS scan of Co 2p, and O 1s regions. In the Co 2p region, two peaks at 779.4 and 794.8 eV are observed, which can be assigned to Co $2p_{3/2}$ and Co $2p_{1/2}$, respectively, of the oxidation state of Co_3O_4. In Fig. S4(b), the O1 s peak is located at 530.1 eV, corresponding to the oxygen species in the Co_3O_4 phase. The XPS results, in conjunction with other aforementioned studies, confirm the formation of Co_3O_4 with normal spinel structure.

Formaldehyde (CH_2O) is a colorless but toxic chemical that is commonly used in building materials and to produce many household products [32]. Materials containing formaldehyde can release formaldehyde gas into the air. Formaldehyde is identified as a probable human carcinogen by U.S. Environmental Protection Agency (EPA), and exposure to formaldehyde at concentrations as low as 0.1 ppm can cause nasal and eye irritation, neurological effects, and increased risk of asthma and/or allergy. Furthermore, high levels of exposure may cause some types of cancers. The high toxicity makes the accurate detection of formaldehyde important. For formaldehyde sensing, various metal oxides have been investigated previously, such as SnO_2, NiO, Fe_2O_3, ZnO, and Co_3O_4 [11,32–42]. Among these metal oxides, Co_3O_4 has shown great promise for the sensitive detection of formaldehyde due to its high catalytic activity [15,40–43].

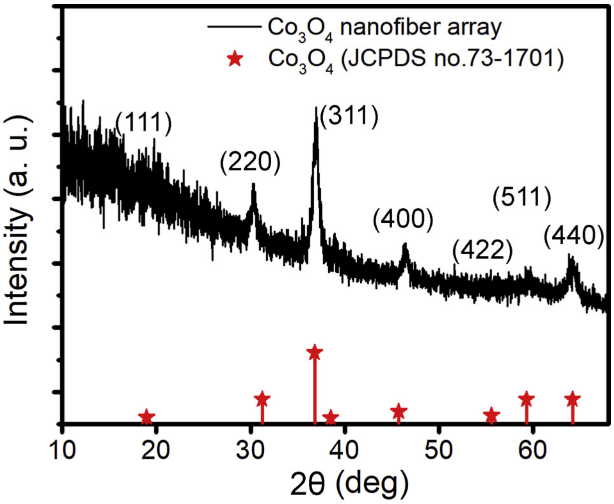

Fig. 5. X-ray diffractogram of as-prepared nanostructured Co_3O_4 network.

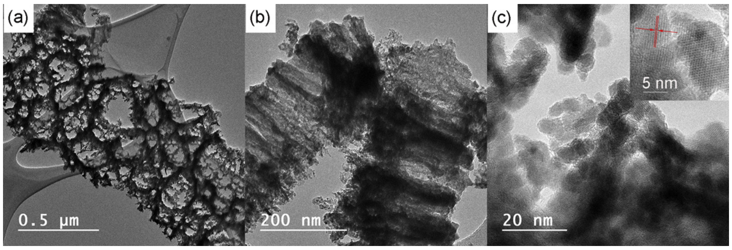

Fig. 4. TEM images of the nanostructured Co_3O_4 network with different magnifications and at different angles (a) top-down view at a low magnification showing the high porous structure; (b) side view at a higher magnification; (c) high resolution TEM image of the nanofibers showing the small grain size; Inset: high magnification TEM image showing the lattice fringes with lattice spacing of 0.47 nm.

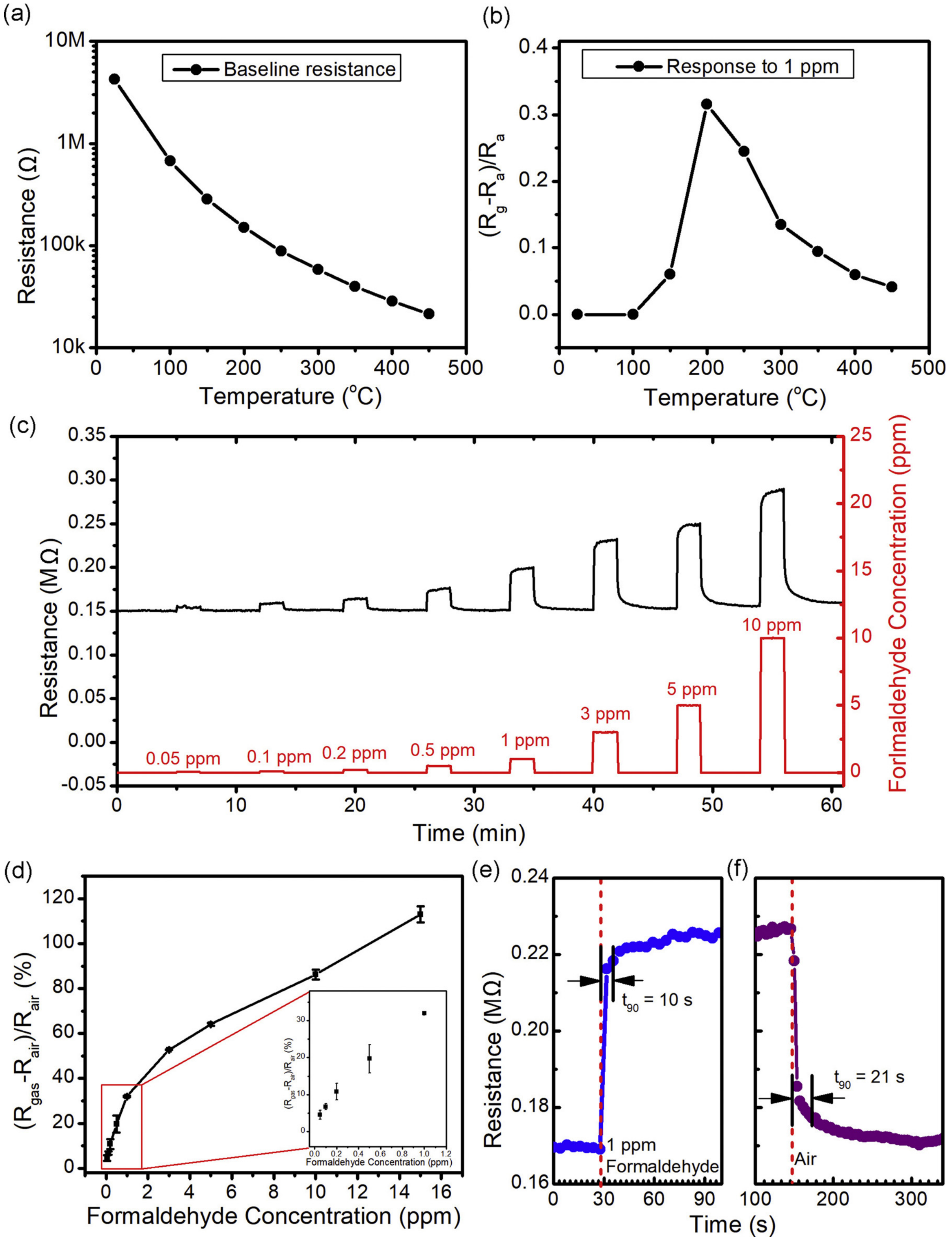

Fig. 6. (a) Baseline resistance of the nanostructured Co_3O_4 sensor at different temperatures. (b) Sensor response to 1 ppm formaldehyde at different microheater temperatures. (c) Real-time resistance change of the sensor to different formaldehyde concentrations at 200 °C. (d) Calculated response versus formaldehyde concentrations. (e–f) Typical response and recovery (t_{90}) to 1 ppm formaldehyde at 200 °C.

The as-prepared nanostructured Co_3O_4 network on microheater platform can be directly used as a gas sensor. As shown in Fig. S5, the IV curve is close to linear at room temperature indicating the good contact between the Co_3O_4 and electrodes. The sensing performance toward formaldehyde is investigated as shown in Fig. 6. It is known that the sensor operating temperature affects both the response and recovery times due to its simultaneous effects on gas adsorption/desorption, diffusion, and reaction rates. Fig. 6(a) shows the baseline resistance of the sensor in air at different temperatures. As can be observed, the baseline resistance decreases with the increasing temperature, which is primarily due to the negative temperature coefficient of resistance (TCR) of the semiconducting metal oxide. Fig. 6(b) shows the effect of temperature on the sensor response towards 1 ppm formaldehyde. Sensor response is defined as the relative percentage change of

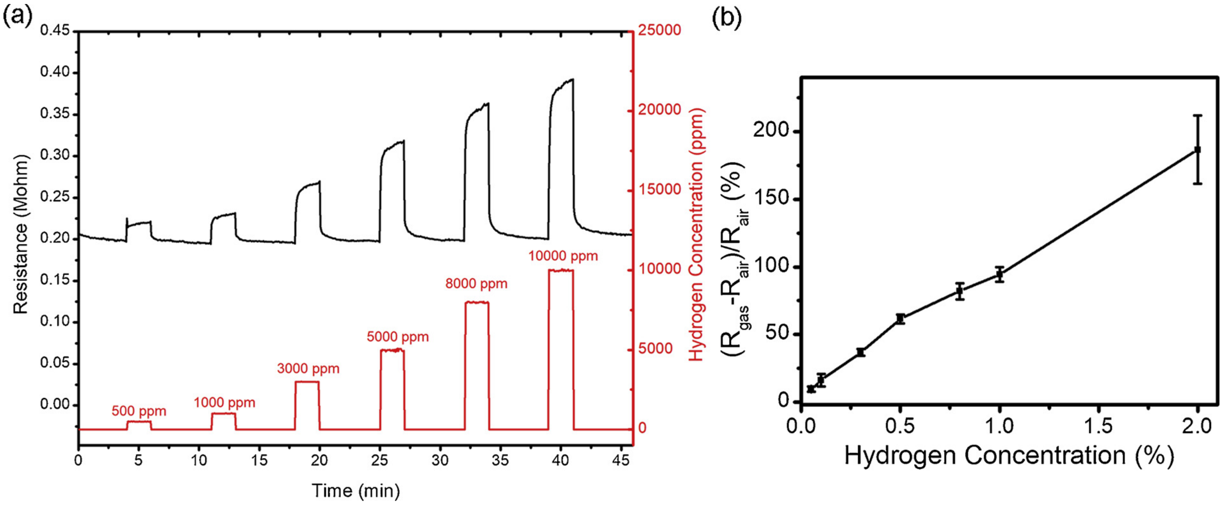

Fig. 7. (a) Real-time resistance change of the sensor to different hydrogen concentrations at 200 °C. (b) Calculated response versus hydrogen concentrations.

resistance, calculated as

$$R\ (\%) = (R_g - R_a)/R_a \tag{1}$$

where R_g and R_a are the resistance of the sensor when exposed to target gas and dry air, respectively.

As can be observed, the sensor response to 1 ppm formaldehyde first increases with increasing temperature, reaches a maximum at 200 °C, and then decreases with further increase in temperature. There are two main oxygen reactions controlling the sensing process which need to be considered to fully understand the effect of working temperature. These two reactions include oxygen adsorption reaction (2) and reaction with formaldehyde (3):

$$O_{2\ g} + 2e^{-} \text{—} > 2(O_{ads})^{-} \tag{2}$$

$$CH_2O + 2(O_{ads})^{-} \text{—} > CO_2 + H_2O + 2e^{-} \tag{3}$$

These equations show that the sensing process is based on two surface-controlled charge transfer reactions, resulting in a change in sensor element resistance. In ambient environment, there will be chemisorbed oxygen species on the metal oxide surface. Depending on the temperature and the surface catalytic activity of the specific metal oxide, chemisorbed oxygen molecules are subsequently converted to $(O_{2\ ads})^{-}$, $(O_{ads})^{-}$ and $(O_{lattice})^{-}$ species via Reaction (2). In this reaction, chemisorbed oxygen molecules capture electrons from metal oxide, resulting in an increase in conductivity for p-type Co_3O_4. When exposed to formaldehyde, the chemisorbed oxygen species react with formaldehyde via Reaction (3), and release electrons back into Co_3O_4, leading to an increase in resistance. The elevated temperatures bring about the following changes: (i) the bonding formed between oxygen [changing from $(O_{2\ ads})^{-}$ to $(O_{ads})^{-}$ and $(O_{lattice})^{-}$] and metal oxide is stronger, resulting in more electrons being trapped via Reaction (2); (ii) the amount of oxygen adsorbed is reduced due to the enhanced desorption; and (iii) the catalytic activity of Co_3O_4 is enhanced as more thermal energy is provided for Reaction (3). At low temperatures, the thermal energy provided is not enough to activate Reaction (3), and thus the response is low and response and recovery are slow. When the temperature is increased, the thermal energy provided enhances the reaction rate and the sensor shows increasing response to formaldehyde. However, when the temperature increases above 200 °C, the desorption of the chemisorbed oxygen and formaldehyde is enhanced more than the reaction rate, leading to a decrease in response with an increased response and recovery time constant.

Fig. 6(c) shows a representative real time sensor resistance change towards different formaldehyde concentrations at 200 °C. When the sensor is exposed to formaldehyde, sensor resistance increases rapidly and reaches a plateau. When the gas is removed, the resistance falls back to its baseline. Both the baseline and sensor response are stable with low noise, which is due to the good contact formed between the nanofiber array and Pt/Ti electrodes. The sensor response increases with the increasing formaldehyde concentration, from 50 ppb to 10 ppm. The lowest concentration considered here, 50 ppb, is well below the threshold value of 0.1 ppm set by the EPA. As 50 ppb is the lowest concentration the testing gas delivery system can reliably deliver, the calculated detection limit of the sensor to formaldehyde is 40 ppb, corresponding to a signal-to-noise threshold value of 3. The high sensitivity of the sensor can be ascribed to the unique nanostructure and small grain size of the nanofiber. As shown in Fig. 6(d), at lower gas concentrations the sensor response increases proportionally with formaldehyde concentration. No significant saturation is observed in the tested gas concentration range, suggesting that the sensor is capable of detecting higher formaldehyde concentrations as well.

In addition to sensitivity, response and recovery times are critical parameters for gas sensing. For many applications, fast response and recovery times are highly desirable. Figs. 6e and f show typical sensor response and recovery to 1 ppm formaldehyde. The response and recovery times to reach 90% of the steady-state signals (t_{90}) are calculated to be 10 and 21 s, respectively, which are much faster than most reported metal oxide-based sensors. The improved response and recovery time may be attributed to the multiscale porosity, which allows for fast diffusion to the active sites.

One of the main drawbacks of metal oxide sensors is their generally poor selectivity. The selectivity of Co_3O_4 -based sensor is investigated. The Co_3O_4 sensor also shows good sensing response towards hydrogen at 200 °C, as shown in Fig. 7. The sensor responds linearly to hydrogen concentrations ranging from 500 to 20,000 ppm with fast response and recovery. To reach the same response as formaldehyde, the concentration of hydrogen must be significantly higher. Fig. 8 compares the sensor responses to a variety of common gases at 200 °C. The sensor shows high response to low concentrations of formaldehyde (1 ppm) but considerably poorer response to 1 ppm NH_3, 1000 ppm CO_2 and 1000 ppm H_2. The observed selectivity may be due to preferential adsorption and reaction of the CH_2O molecules at the defect sites on the Co_3O_4 surface. It is well known that the selectivity of metal oxides can be tuned by changing composition. Considering the flexibility afforded by the presented fabrication method, the sensing performance can likely be easily optimized for various gases and different applications, e.g., by changing or selecting the metal precursor combination. This exploits the large selection of metal salts available.

The effect of relative humidity on the gas-sensing properties of the nanostructured Co_3O_4 sensor is also investigated. Fig. S6(a) compares

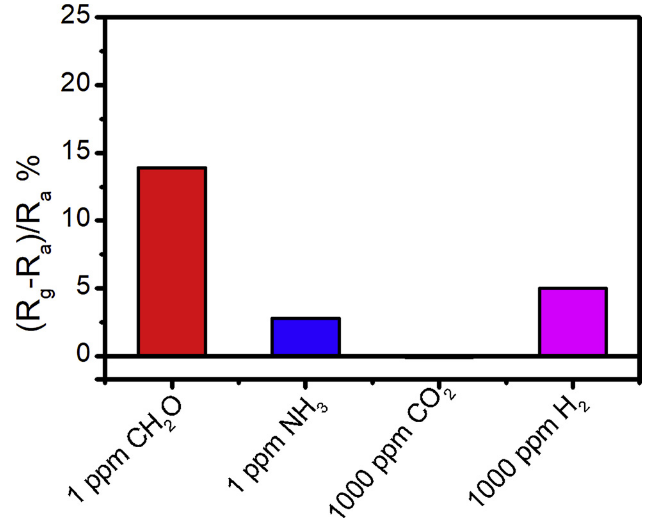

Fig. 8. Selectivity of the nanostructured Co_3O_4 based low power sensor.

the sensor response to different formaldehyde concentrations in dry air and 30% relative humidity. The baseline resistance increases with increasing relative humidity (Fig. S6 (a–c)). Adsorbed water is acting as an electron donor upon forming hydroxyl groups ($-OH^-$) on the sensor surface and thus increasing the sensor resistance. It was found that the sensor response decreases with increase in relative humidity level at both 200 °C and 400 °C (Fig. S6 (c–d)). In high humidity environment, water molecules compete with O_2 at the adsorption sites, resulting in less surface oxygen species, which negatively affects the surface reaction between formaldehyde and surface oxygen species, thus lower sensor response. However, the sensor response is fully restored as the relative humidity level returns to 0% again, indicating the temporary effect of humidity rather than a permanent “poisoning” effect.

The sensors fabricated by the above method are highly reproducible and stable. The responses of the sensors fabricated in the same process batch (on the same chip) are within 15% of the average. The differences in responses of sensors from different batches, fabricated with the same parameters, are within 40% of the average and the sensors also exhibit good stability. The baseline resistance remains constant (less than 5% change) during 20 h of continuous operation. The response of the sensor decreases by less than 15% after 20 days. The stability can likely be further improved by doping, or by using a combination of different metal oxides.

3. Conclusion

We have presented a flexible and facile method for the fabrication of high-performance gas sensors through plasma assisted on-chip synthesis of highly porous nanostructured metal oxide network on a low power microheater platform. The nanofibers created by this method are porous and interconnected, and hence ideal for gas sensing. Various metal oxide fibers, such as Co_3O_4, NiO, and SnO_2, have been fabricated to demonstrate the validity and flexibility of this method. Taking nanostructured Co_3O_4 network as an example material, the resulting sensor shows high sensitivity and selectivity to formaldehyde with fast response and recovery. This facile and versatile fabrication strategy provides a way to produce low power sensors with tunable sensing performance depending on the choice and composition of metal oxides, and has the potential for low cost mass production.

4. Experimental section

4.1. Microheater fabrication

The fabrication process and characterization for the silicon carbide microheater are described in detail in our previous publications [9,10]. Briefly, 130 nm doped polycrystalline cubic 3C-SiC (sheet resistivity of 5700 Ω/square) is patterned and encapsulated in 200 nm low-stress silicon nitride (LSN) film. The sensing electrodes and microheater contacts are composed of 10 nm titanium and 90 nm platinum. Finally, the wafers are etched with KOH from the backside to remove the silicon under the microheaters, leaving only the thin silicon nitride membrane. The wafer is diced into 3.5×3.5 mm^2 chips, each of which has four individual microheaters.

4.2. Sensor device fabrication

The aqueous precursor solution is prepared by dissolving metal salts in a water based PVA solution. First, PVA is added to water under vigorous stirring for 3 h at room temperature. The solution is then heated to 100 °C and stirred for 5 h to form a clear solution. Subsequently, metal salts are added to the solution in specific ratio to PVA under vigorous stirring. The solution is cooled to room temperature and left overnight to remove bubbles in the solution.

The prepared solution is spin-coated onto the microheater chip at 3000 rpm for 60 s (the metal pads on microheater chip for wire bonding are covered by tape before spin-coating). By adjusting the spin speed, the desired fiber length can be controlled. The chip is then baked at 80 °C for 10 min on a hotplate to evaporate water in the film. Afterwards, the chip is exposed to oxygen plasma (300 W, 100 sccm) for 300 s in a plasma etcher and the nanofiber array is formed. The chip is subsequently annealed in a tube furnace at 500 °C in air for 2 h. The annealing also can be done using the microheater itself to achieve the selective growth of nanofibers on microheater site only, followed with a hot water wash on the rest of the chip to remove polymer nanofibers.

4.3. Materials characterization

The morphology of the samples is characterized using field-emission scanning electron microscopy (FESEM, JEOL 2100 F), and transmission electron microscopy (TEM, JEOL 2010). The crystal structure is characterized using X-ray diffraction (XRD; Bruker AXS d8 Discover GADDS) employing radiation from a Co target (Ka, $\lambda = 0.179$ nm).

4.4. Sensor device testing

The sensor chip is wire-bonded into a 14-pin ceramic package and then placed within a gas flow chamber with a volume of 1 cm^3 for electrical and gas sensing test. The sensor is exposed to various gases, namely formaldehyde (Praxair, 20 ppm in N_2), CO_2 (Praxair, 2000 ppm in N_2), NH_3 (Praxair, 10 ppm in N_2), and hydrogen (Praxair, 5% in N_2) using a LabView-controlled gas delivery system. The total flow rate is controlled at 300 sccm. The electric measurement of the sensor is conducted by a Keithley 2602 source-meter controlled by Zephyr, an open-source Java-based instrument and control and measurement software suite. The sensor measurement is taken by continuously applying a bias voltage and recording the current, which is used to calculate the resistance, R. All the data including gas flow information, temperature, humidity, and electric measurement information are collected by Zephyr.

Acknowledgements

This work was supported primarily by the Director, Office of Science, Office of Basic Energy Sciences, Materials Sciences and Engineering Division, of the U.S. Department of Energy under Contract

No. DE-AC02-05-CH11231, within the sp2-Bonded Materials Program (KC2207), which provided for design of the project, synthesis of the sensor material, and SEM characterization of the nanofibers. Support was also provided by the Director, Office of Science, Office of Basic Energy Sciences, Materials Sciences and Engineering Division, of the U.S. Department of Energy under Contract No. DE-AC02-05-CH11231, within the van der Waals Heterostructures program (KCWF16), which provided for microheater fabrication. Structural characterization was conducted at the Molecular Foundry, which is supported by the Office of Science, Office of Basic Energy Sciences, of the U.S. Department of Energy under Contract No. DE-AC02- 05CH11231. Additional support was provided by the National Science Foundation under Grant No. DMR-1807233 which provided for TEM characterization, under Grant No. 1542741 which provided for gas response testing, and under Grant No. 1444950 which provided for microheater design and fabrication. ST acknowledges support from a National Science Foundation Graduate Research Fellowship. The authors thank Dr. Anna Harley-Trochimczyk for assistance with the polysilicon carbide microheater design and fabrication.

Appendix A. Supplementary data

Supplementary material related to this article can be found, in the online version, at doi:https://doi.org/10.1016/j.snb.2019.127067.

References

[1] N. Yamazoe, N. Miura, Environmental gas sensing, Sensors Actuators B. Chem. 20 (1994) 95–102, https://doi.org/10.1016/0925-4005(93)01183-5.

[2] G. Korotcenkov, Handbook of gas sensor materials: properties, Advantages and Shortcomings for Applications. Volume 2, New Trends and Technologies, (2014), https://doi.org/10.1007/978-1-4614-7388-6.

[3] A. Kaushik, R. Kumar, R.D. Jayant, M. Nair, Nanostructured gas sensors for health care: an overview, J. Pers. Nanomedicine. (2015), https://doi.org/10.1021/cr400659h.

[4] F. Röck, N. Barsan, U. Weimar, Electronic nose: current status and future trends, Chem. Rev. (2008), https://doi.org/10.1021/cr068121q.

[5] B. Roussel, GAS SENSOR TECHNOLOGY AND MARKET, (2016) http://www.yole.fr/Gas_Sensor_ConsumerMarket.aspx#.XDPQTy2ZMWo.

[6] H. Hejun, R. Bogue, MEMS sensors: past, present and future, Sens. Rev. 27 (2007) 7–13, https://doi.org/10.1108/02602280710729068.

[7] S. Semancik, R.E. Cavicchi, M.C. Wheeler, J.E. Tiffany, G.E. Poirier, R.M. Walton, J.S. Suehle, B. Panchapakesan, D.L. DeVoe, Microhotplate platforms for chemical sensor research, Sens. Actuators, B Chem. 77 (2001) 579–591, https://doi.org/10.1016/S0925-4005(01)00695-5.

[8] A. Harley-Trochimczyk, J. Chang, Q. Zhou, J. Dong, T. Pham, M.A. Worsley, R. Maboudian, A. Zettl, W. Mickelson, Catalytic hydrogen sensing using microheated platinum nanoparticle-loaded graphene aerogel, Sens. Actuators, B Chem. 206 (2015) 399–406, https://doi.org/10.1016/j.snb.2014.09.057.

[9] A. Harley-Trochimczyk, A. Rao, H. Long, A. Zettl, C. Carraro, R. Maboudian, Low-power catalytic gas sensing using highly stable silicon carbide microheaters, J. Micromech. Microeng. 27 (2017), https://doi.org/10.1088/1361-6439/aa5d70.

[10] A. Rao, H. Long, A. Harley-Trochimczyk, T. Pham, A. Zettl, C. Carraro, R. Maboudian, In situ localized growth of ordered metal oxide hollow sphere array on microheater platform for sensitive, ultra-fast gas sensing, ACS Appl. Mater. Interfaces 9 (2017) 2634–2641, https://doi.org/10.1021/acsami.6b12677.

[11] H. Long, A. Harley-Trochimczyk, T. He, T. Pham, Z. Tang, T. Shi, A. Zettl, W. Mickelson, C. Carraro, R. Maboudian, In situ localized growth of porous tin oxide films on low power microheater platform for low temperature CO detection, ACS Sens. 1 (2016) 339–343, https://doi.org/10.1021/acssensors.5b00302.

[12] M.E. Franke, T.J. Koplin, U. Simon, Metal and metal oxide nanoparticles in chemiresistors: Does the nanoscale matter? Small 2 (2006) 36–50, https://doi.org/10.1002/smll.200500261.

[13] G. Korotcenkov, Metal oxides for solid-state gas sensors: What determines our choice? Mater. Sci. Eng. B Solid-State Mater. Adv. Technol. 139 (2007) 1–23, https://doi.org/10.1016/j.mseb.2007.01.044.

[14] J.H. Lee, Gas sensors using hierarchical and hollow oxide nanostructures: overview, Sens. Actuators, B Chem. 140 (2009) 319–336, https://doi.org/10.1016/j.snb.2009.04.026.

[15] H. Long, A. Harley-Trochimczyk, S. Cheng, H. Hu, W.S. Chi, A. Rao, C. Carraro, T. Shi, Z. Tang, R. Maboudian, Nanowire-assembled hierarchical ZnCo2O4microstructure integrated with a low-power microheater for highly sensitive formaldehyde detection, ACS Appl. Mater. Interfaces 8 (2016) 31764–31771, https://doi.org/10.1021/acsami.6b11054.

[16] H. Long, A. Harley-Trochimczyk, T. Pham, Z. Tang, T. Shi, A. Zettl, C. Carraro, M.A. Worsley, R. Maboudian, High surface area MoS2/Graphene hybrid aerogel for ultrasensitive NO2Detection, Adv. Funct. Mater. 26 (2016) 5158–5165, https://doi.org/10.1002/adfm.201601562.

[17] U. Dibbern, A substrate for thin-fii gas sensors in microelectronic technology, Sens. Actuators B Chem. 2 (1990) 63–70.

[18] J.S. Suehle, R.E. Cavicchi, M. Gaitan, S. Semancik, Tin oxide gas sensor fabricated using CMOS micro-hotplates and in-situ processing, IEEE Electron Device Lett. (1993), https://doi.org/10.1109/55.215130.

[19] Po-Chiang Chen, Guozhen Shen, Chongwu Zhou, Chemical sensors and electronic noses based on 1-D metal oxide nanostructures, IEEE Trans. Nanotechnol. 7 (2008) 668–682, https://doi.org/10.1109/TNANO.2008.2006273.

[20] J. Kukkola, M. Mohl, A.R. Leino, G. Tóth, M.C. Wu, A. Shchukarev, A. Popov, J.P. Mikkola, J. Lauri, M. Riihimäki, J. Lappalainen, H. Jantunen, K. Kordás, Inkjet-printed gas sensors: metal decorated WO3nanoparticles and their gas sensing properties, J. Mater. Chem. 22 (2012) 17878–17886, https://doi.org/10.1039/c2jm32499g.

[21] D. Kim, Y. Jeong, K. Song, S.K. Park, G. Cao, J. Moon, Inkjet-printed zinc tin oxide thin-film transistor, Langmuir. 25 (2009) 11149–11154, https://doi.org/10.1021/la901436p.

[22] E. Tekin, P.J. Smith, U.S. Schubert, Inkjet printing as a deposition and patterning tool for polymers and inorganic particles, Soft Matter 4 (2008) 703–713, https://doi.org/10.1039/b711984d.

[23] W. Shen, Y. Zhao, C. Zhang, The preparation of ZnO based gas-sensing thin films by ink-jet printing method, Thin Solid Films 483 (2005) 382–387, https://doi.org/10.1016/j.tsf.2005.01.015.

[24] Z. Nie, E. Kumacheva, Patterning surfaces with functional polymers, Nat. Mater. 7 (2008) 277–290, https://doi.org/10.1038/nmat2109.

[25] S. Shin, S.W. Kim, J.H. Jang, J.B. Kim, A simple maskless process for the fabrication of vertically aligned high density hematite and graphene/magnetite nanowires, J. Mater. Chem. C. 5 (2017) 1313–1320, https://doi.org/10.1039/c6tc05162f.

[26] H. Long, T. Pham, A. Yan, Z. Guo, H. Ishida, W. Shi, S. Turner, S.M. Gilbert, A. Zettl, Wafer-scale on-chip synthesis and field emission properties of vertically aligned boron nitride based nanofiber arrays, Appl. Phys. Lett. 114 (2019) 093101, , https://doi.org/10.1063/1.5079655.

[27] S. Jiang, T. Shi, Y. Gao, H. Long, S. Xi, Z. Tang, Fabrication of a 3D micro/nano dual-scale carbon array and its demonstration as the microelectrodes for supercapacitors, J. Micromech. Microeng. 24 (2014), https://doi.org/10.1088/0960-1317/24/4/045001.

[28] E. Wohlfart, J.P. Fernández-Blázquez, E. Knoche, A. Bello, E. Pérez, E. Arzt, A. Del Campo, Nanofibrillar patterns by plasma etching: the influence of polymer crystallinity and orientation in surface morphology, Macromolecules 43 (2010) 9908–9917, https://doi.org/10.1021/ma101889s.

[29] H. Fang, W. Wu, J. Song, Z.L. Wang, Controlled growth of aligned polymer nanowires, J. Phys. Chem. C. 113 (2009) 16571–16574, https://doi.org/10.1021/jp907072z.

[30] S. Jiang, T. Shi, X. Zhan, S. Xi, H. Long, B. Gong, J. Li, S. Cheng, Y. Huang, Z. Tang, Scalable fabrication of carbon-based MEMS/NEMS and their applications: a review, J. Micromech. Microeng. 25 (2015), https://doi.org/10.1088/0960-1317/25/11/113001.

[31] J.R. Morber, X. Wang, J. Liu, R.L. Snyder, Z.L. Wang, Wafer-level patterned and aligned polymer nanowire/ micro- and nanotube arrays on any substrate, Adv. Mater. 21 (2009) 2072–2076, https://doi.org/10.1002/adma.200803648.

[32] https://www.epa.gov/formaldehyde, (n.d.). https://www.epa.gov/formaldehyde (accessed January 9, 2018).

[33] T. Kida, T. Doi, K. Shimanoe, Synthesis of monodispersed SnO2 nanocrystals and their remarkably high sensitivity to volatile organic compounds, Chem. Mater. 22 (2010) 2662–2667, https://doi.org/10.1021/cm100228d.

[34] A.D. James, D. Kristin, A.R. Terry, NiO thin films formaldehyde gas sensor, Sens. Actuators B Chem. 80 (2001) 106–115.

[35] C.Y. Lee, C.M. Chiang, Y.H. Wang, R.H. Ma, A self-heating gas sensor with integrated NiO thin-film for formaldehyde detection, Sens. Actuators B Chem. 122 (2007) 503–510, https://doi.org/10.1016/j.snb.2006.06.018.

[36] P. Lv, Z.A. Tang, J. Yu, F.T. Zhang, G.F. Wei, Z.X. Huang, Y. Hu, Study on a micro-gas sensor with SnO2-NiO sensitive film for indoor formaldehyde detection, Sens. Actuators B Chem. 132 (2008) 74–80, https://doi.org/10.1016/j.snb.2008.01.018.

[37] P.R. Chung, C.T. Tzeng, M.T. Ke, C.Y. Lee, Formaldehyde gas sensors: a review, Sensors (Switzerland). 13 (2013) 4468–4484, https://doi.org/10.3390/s130404468.

[38] J. Xu, X. Jia, X. Lou, G. Xi, J. Han, Q. Gao, Selective detection of HCHO gas using mixed oxides of ZnO/ZnSnO3, Sens. Actuators B Chem. 120 (2007) 694–699, https://doi.org/10.1016/j.snb.2006.03.033.

[39] S. Liu, Z. Wang, H. Zhao, T. Fei, T. Zhang, Ordered mesoporous Co3O4for high-performance toluene sensing, Sens. Actuators B Chem. 197 (2014) 342–349, https://doi.org/10.1016/j.snb.2014.03.007.

[40] S. Deng, X. Liu, N. Chen, D. Deng, X. Xiao, Y. Wang, A highly sensitive VOC gas sensor using p-type mesoporous Co3O4 nanosheets prepared by a facile chemical coprecipitation method, Sens. Actuators B Chem. 233 (2016) 615–623, https://doi.org/10.1016/j.snb.2016.04.138.

[41] J.Y. Kim, N.-J. Choi, H.J. Park, J. Kim, D.-S. Lee, H. Song, A hollow assembly and its three-dimensional network formation of single-crystalline Co3O4 nanoparticles for ultrasensitive formaldehyde gas sensors, J. Phys. Chem. C. 118 (2014) 25994–26002, https://doi.org/10.1021/jp505791v.

[42] S. Bai, J. Guo, X. Shu, X. Xiang, R. Luo, D. Li, A. Chen, C.C. Liu, Surface functionalization of Co3O4hollow spheres with ZnO nanoparticles for modulating sensing properties of formaldehyde, Sens. Actuators B Chem. 245 (2017) 359–368, https://doi.org/10.1016/j.snb.2017.01.102.

[43] S. Bai, H. Liu, J. Sun, Y. Tian, R. Luo, D. Li, A. Chen, Mechanism of enhancing the formaldehyde sensing properties of Co_3O_4via Ag modification, RSC Adv. 5 (2015)

48619–48625, https://doi.org/10.1039/c5ra05772h.

Hu Long is postdoctoral researcher, working with Prof. Alex Zettl in the Department of Physics at the University of California, Berkeley. He received his bachelor's degree and Ph.D. from Huazhong University of Science and Technology in Wuhan, China. His research is focused on the development of low power sensors.

Carlo Carraro is an adjunct professor in the Department of Chemical and Biomolecular Engineering at the University of California, Berkeley. He received his bachelor's degree from the University of Padua, Italy, and his Ph.D. from the California Institute of Technology in Pasadena, California. His research interests are in the physics of surfaces and in novel thin film materials and processes.

Roya Maboudian is a Professor of chemical engineering at the University of California, Berkeley and co-director of the Berkeley Sensor & Actuator Center. She received her Ph.D. in applied physics from California Institute of Technology. Her research interests are in the areas of surface/interfacial science and engineering of micro-/nanosystems, and thin-film science and technology.

Alex Zettl is a Professor of physics the University of California, Berkeley and a Senior Scientist at the Lawrence Berkeley National Laboratory. He received his Ph.D. in experimental condensed matter physics from the University of California, Los Angeles. His research is focused on investigating electronic, magnetic and mechanical properties of nanoscale materials.